Effect of Constraint on Stretch Zone Width and Fracture Toughness of Structural Steels

N. Narasaiah* M. Tarafder, S. Sivaprasad, S. Tarafder
National Metallurgical Laboratory, CSIR, Jamshedpur 831007, India.

Abstract

Fracture toughness obtained with standard procedures of analysis is a function of the constraint condition attending a crack tip. In recent times, the width of the stretch zone that develops prior to the initiation of ductile fracture has been of interest. It is instructive to observe the effect of variation of constraint on stretch zone formation. The stretch zone width can be employed as an effective marker for identifying fracture toughness from resistance curves. From this premise, it is important to study the variation of fracture toughness determined thus with variation of constraint.

In this work, the effect of constraint on stretch zone width and fracture toughness determined using it have been examined for two pressure vessel and piping steels. This has been contrasted with the toughness metrics obtained through standard procedure, and major deviations noted. Of particular significance is the apparent independence of stretch zone fracture toughness with constraint.

1. Introduction

Determination of initiation toughness in ductile materials is not straightforward, unlike in brittle materials, where the point of crack initiation is easily detectable due to sharp changes in the load carrying capacity of specimens being tested. The matter may be further complicated because of to variation of constraint attending crack tips. Fracture behaviour of ductile materials is usually characterized by elastic-plastic fracture parameters such as the *J*-integral, stretch zone width, crack tip opening displacement etc. The variations in these parameters with variation in constraint are often difficult to rationalize, particularly from the point of view that they are employed to represent material behaviour that are deemed to be universal, largely independent of test and specimen parameters. Often, the fracture resistance of materials obtained from testing standard specimens is not applicable to the fracture of components made of that material due to the difference in the constraint or triaxiality conditions at the tip of the crack in the

* Corresponding author: Tel.: +91 657 2271709; Fax: +91 657 2270527; E-mail: narasaiahn@yahoo.co.in

two cases [1]. An attempt has been made to understand the nature of variation of fracture resistance parameters with change in crack length (i.e. with variation of constraint) in two pressure vessel piping materials. The suitability of the parameters to represent the fracture toughness of materials, irrespective of the constraint condition, to which cracks in them are subjected, is discussed.

In ductile materials, fatigue precrack blunts on the application of load to accommodate plastic strains arising out of the local deformation processes at the crack tip. On continuation of loading, the blunting at the crack tip increases and reaches a limiting size, governed by the deformation capacity of the material, and further initiates a fracture (ductile crack) at its tip. On a ductile fracture surface, crack tip blunting is manifested as a featureless region known as the stretch zone. The stretch zone that forms during the process of ductile fracture can be thought of as a frozen imprint of the state of deformation at the instant of the critical event of ductile crack extension. Its extent can thus be used as a marker to indicate the corresponding fracture toughness parameter from the experimental resistance curve [2-5]. The effect of variation of constraint on the fracture toughness metrics thus determined has also been investigated in the present work.

2. Material and experimental details

The materials selected for this investigation were 20MnMoNi55 and SA333 steels. The 20MnMoNi55 steel was in the form of blanks and the SA333 was in the form of pipe. The nominal composition of both the materials is given in Table 1. Figure 1 shows the typical microstructures of the investigated steels. The SA333 steel consists of banded pearlite in a ferritic matrix, whereas in the 20MnMoNi55 steel pearlite is distributed uniformly in the ferritic matrix. Table 2 lists the mechanical properties of the materials obtained from standard tensile tests at room temperature. The tensile flow curves of both the steels exhibited prominent yield-point effect.

Table 1 Compositions of investigated steels (in weight percentage).

Material	**Elements**									
	C	**Mn**	**Si**	**P**	**S**	**Mo**	**Cr**	**Ni**	**V**	**N**
SA333	0.14	0.9	0.25	0.016	0.018	--	0.08	0.05	<0.01	0.01
20MnMoNi55	0.2	1.25	0.3	--	0.005	0.5	0.17	0.6	--	--

Table 2 Tensile parameters of investigated steels at room temperature

Material.	YS (MPa)	UTS (MPa)	e_u (%)	e_t (%)	RA (%)
SA333	314.6	504.1	16.80	29.30	73.8
20MnMoNi55	489.9	620.5	9.51	23.04	68.65

YS: Yield Strength, UTS: Ultimate Tensile Strength, e_u: Uniform elongation, e_t: Total elongation, RA: Reduction in Area

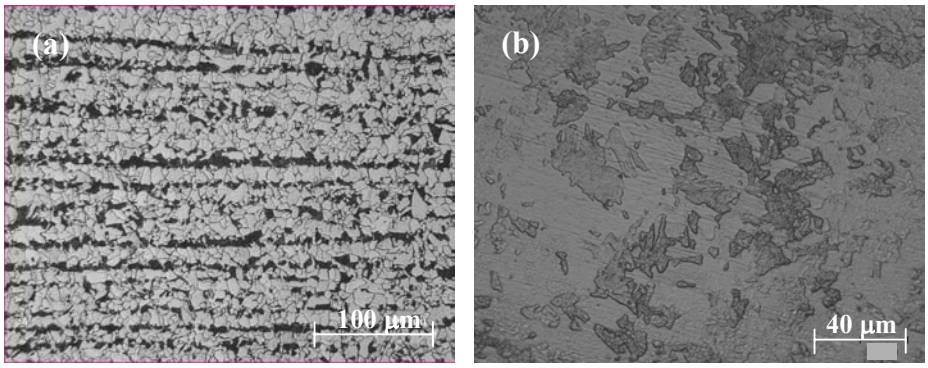

Fig.1 Typical microstructures of the investigated steels; (a) SA333 steel; (b) 20MnMoNi55 steel.

Single-edge notched bend (SENB) specimens, of 20mm thickness (B) and 50mm width (W), were employed for carrying out monotonic single specimen $J - R$ tests at room temperature. For studying constraint effects on ductile fracture behaviour, SENB specimen geometry was preferred to avoid the distortion that occur at the loading holes of the compact tension (CT) geometry at lower initial crack lengths. All specimens were equipped with integral knife-edges on their front face for compliance based crack length measurement, and were side-grooved after fatigue pre-cracking to ensure planar fracture. Specimens were fatigue pre-cracked under decreasing ΔK envelopes in servo-hydraulic testing systems interfaced to computers for test control and data acquisition. Pre-cracks (a) of various extents were incorporated in the specimens to vary the crack tip constraint. In this paper, the precise quantification of constraint condition has not been reported.

The single-specimen technique was employed for generating $J - R$ curves as per the procedures laid down in ASTM standard E1820 [6]. The loading scheme for this technique consisted of ramping pre-cracked specimens at a rate of $3\text{x}10^{-3}$ mm/s through constant incremental displacements, followed by unloading and then reloading through 50% of the incremental displacement at the same rate, and repeating the sequence 45 to 50 times till substantial crack extension had taken place through ductile tearing. The typical load-displacement records that results due to implementation of this scheme for 20MnMoNi55 steel at two a/W ratios are shown in Fig. 2.

The crack length (a) at each instance of unloading was calculated from the elastic compliance (C) of the unloading curve using compliance crack length relations of the form;

$$\frac{a}{W} = f(u),\ u = \frac{1}{\sqrt{EB_{eff}C} + 1} \qquad (1)$$

where, E is the elastic modulus, and f is a polynomial function. The energy parameter J for the instant of i^{th} unloading was calculated incrementally using;

$$J_i = \frac{K_i^2(1-\nu^2)}{E'} + J_{pl(i)} \qquad (2a)$$

$$J_{pl(i)} = \left(J_{pl(i-1)} + \frac{\eta_{(i-1)}(A_{pl(i)}-A_{pl(i-1)})}{b_{(i-1)}B_N}\right)\left(1 - \frac{\gamma_{(i-1)}(a_i-a_{(i-1)})}{b_{(i-1)}}\right) \qquad (2b)$$

where, $A_{pl(i)}$-$A_{pl(i-1)}$ = incremental plastic area; b_i=(W-a_i)

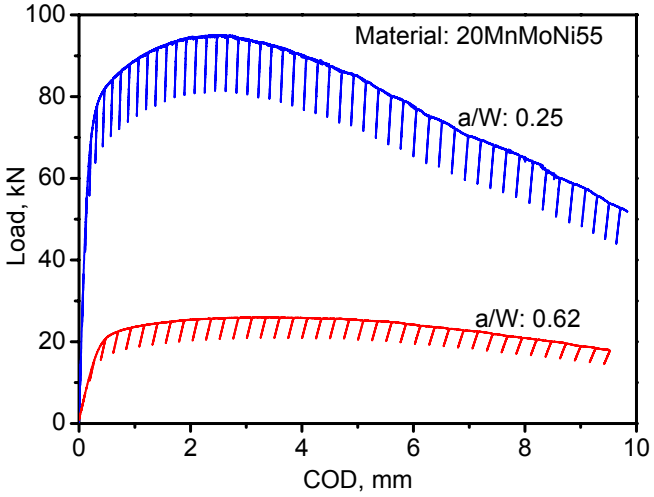

Fig.2 Load-displacement records obtained during J-R testing at different *a/W* ratios for 20MnMoNi55 steel.

In the above equations, K_i is the stress intensity factor, calculated from the instantaneous load $P_{(i)}$ and the crack length $a_{(i)}$; ν is the Poisson's ratio; η and γ are geometry and crack length dependent factors; and B_N is the net specimen thickness obtained after side grooving. The second term in eq. (2b) represents the correction proposed by James and Richard [7] to account for crack extension in the loading step. The factors η and γ in equation (2b) are strongly dependent on crack length and were obtained from relations given by Sumpter [8]. This is necessary when pre-crack lengths are varied through a large range in order to study constraint effects on ductile fracture.

The load, displacement and crack mouth opening displacement (CMOD) data obtained from ductile fracture tests were analysed post-test, employing a software to obtain a set of J and crack extension (Δa) data pairs to construct the $J - R$ curve. The software incorporated iterative procedures to obtain the experimental blunting line slope m, the power law representation of the tearing part of the

resistance curve, and the adjusted initial crack length a_{oq}. This ensured that subjectivity in determination of critical parameters such as the fracture toughness J_i, obtained at the departs of the power law tearing curve from the blunting line, or the critical fracture toughness J_c, identified from the point where an offset of the blunting line at Δa = 0.2 mm intersects the tearing curve, was eliminated.

Fractured surfaces carefully extracted from the tested specimens were placed on the stage of the SEM, and the plane of fracture was aligned to be normal to the electron beam. At this 0^o tilt position, stretch features were recorded at a sufficiently high magnification to be able to identify local features within the stretch zone, while ensuring that the whole width of the stretch zone was contained in the field of view. Care was taken to obtain a good contrast, so that stretch zone limits could be demarcated easily. The stretch zone boundaries were traced on captured SEM images and approximately 25 measurements were made for each of the two fracture surfaces obtained from a specimen. Large number of measurements was made so that the variation in stretch zone dimension across the specimen thickness is rectified. The average of these measurements was taken as the representative stretch zone width. The stretch zone dimensions that were determined from SEM images have been used in conjunction with the experimentally derived *J-R* curve to obtain a value of the ductile fracture toughness J_{SZW}. A comparison of J_{SZW} (estimated from stretch zone width) with J_i and J_c (estimated following ASTM standard) has been carried out.

3. Results and discussions

The typical load-displacement records obtained during *J-R* testing at *a/W* ratios of 0.25 and 0.62 for 20MnMoNi55 steel are given Fig.2. It may be observed from the plots that specimens have been loaded to beyond their maximum load capacity. From the fractured surfaces of tested specimens it was observed that good amount of tearing had taken place. To understand the response of variation of constraint, *J–R* curves were obtained from load-displacements records of tested specimens precracked to *a/W* in the range of 0.25–0.75 in steps of approximately 0.1. From the *J-R* curves of the tested specimens, using standard procedures of the ASTM standard E-1820 [6], the fracture toughness parameters J_c and J_i were obtained. It could not be qualified as J_{Ic} due to size requirements of the ASTM standard not being fulfilled.

The effect of increasing initial crack length on *J-R* curves is summarized in Fig. 3 for SA333 and 20MnMoNi55 steels. From Fig.3, it may be noted that decreased initial crack lengths *(a/W)*, the slope of J-R curve increases, and this is more prominent in case of 20MnMoNi55 steel. It is observed that the effect of variation of crack tip constraint on the *J-R* curves of SA333 steel is not very significant.

James and Richard [7] have shown that fracture resistance curves exhibit a lowering with increase in the specimen crack length. This behaviour has been attributed to the increase of crack tip constraint with increasing crack length. However, at deeper crack lengths, a recovery of the *R*-curve has been observed. This has been shown to originate from the fact that the crack tip constraint saturates at $a/W \geq 0.5$, after which, with further increase in crack length, far field stresses are superimposed on the crack tip stress field, and result in a drastic loss of constraint.

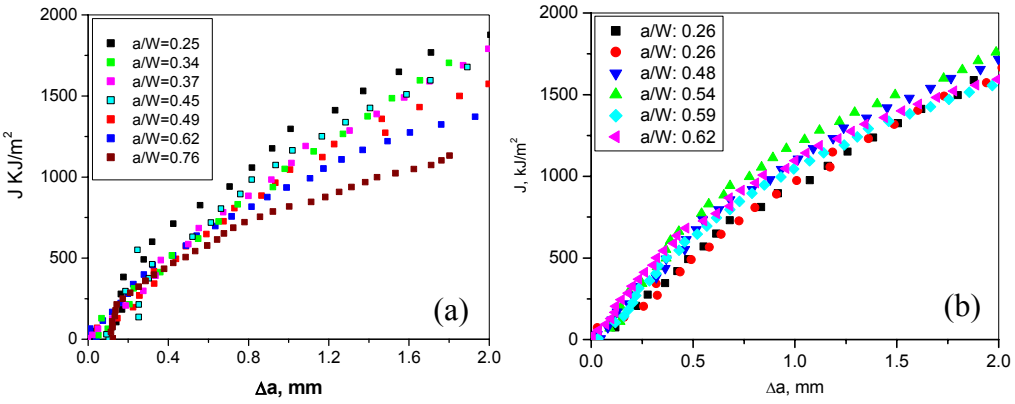

Fig. 3 J-R curves for different a/W ratios of specimens of (a) 20MnMoNi55 and (b) SA333 steels.

The trends observed in the variation of J_i and J_c with change in a/W, as determined from the *J-R* curve, are shown in Fig. 4. It may be noted that both J_i and J_c show an exponentially decreasing and saturating trend with increase in a/W for 20MnMoNi55 steel. In case of SA333 steel, the trends seems to increase up to $a/W \approx 0.45$-0.55 before decreasing on further increase of a/W. The exponentially decreasing trend for fracture toughness with increasing crack length (and hence constraint), as observed for 20MnMoNi55 steel, has been observed earlier [9-11] The behaviour exhibited by SA333 steel is thought to be due to a additional loss of constraint at intermediate crack lengths ($0.45 \leq a/W \leq 0.6$) because of uncontained yielding of the ligament.

Typical stretch zones of tested specimens of 20MnMoNi55 and SA333 steels are shown in Fig. 5. Stretch zone formation is very prominent and starting/ending points are clearly discernible in 20MnMoNi55 steel. In the SA333 steel, it was observed that the ductile fracture surface consists of a series of ridges with the valley between the ridges exhibiting stretch zone features. The first expanse of stretch features was considered as the width of the stretch zone for this material.

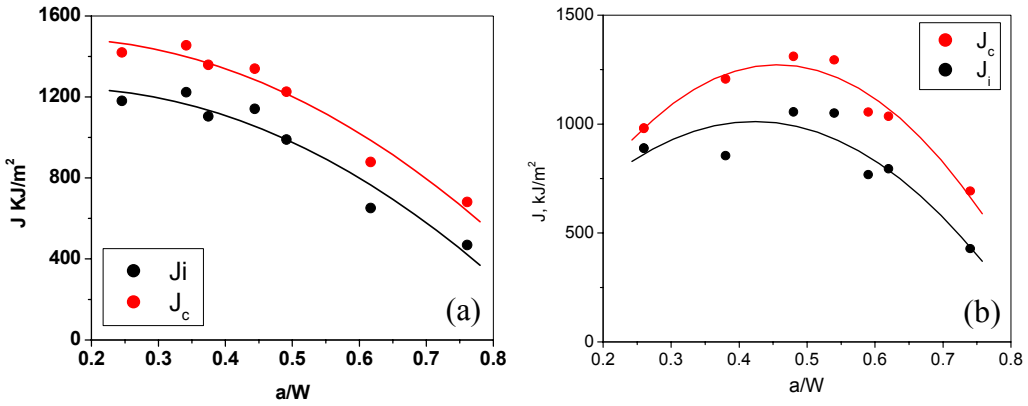

Fig.4 Variation of J_i and J_c with change in initial crack length in (a) 20MnMoNi55 and (b) SA333 steels.

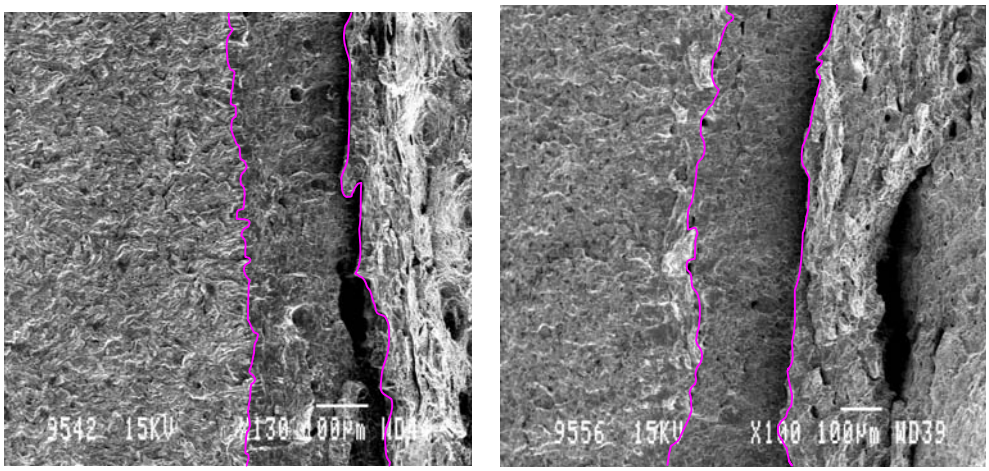

Fig. 5 Typical stretch zone images of tested specimens of (a) 20MnMoNi55 and (b) SA333 steels.

The stretch zone dimensions that were determined for the specimens with various *a/W* in the two materials have been used in conjunction with the experimentally derived *J-R* curve to obtain a value of the *J* corresponding to stretch zone width (J_{SZW}). The J_{SZW} is identified at $\Delta a = \Delta a_{szw}$, the width of stretch zone. The correlation of J_{SZW}, critical toughness, (J_C) and initiation toughness, (J_i), has been examined with a view to ascertain the applicability of the stretch zone dimension for measurement of fracture toughness. It is re-iterated that J_i is the value at intersection of blunting line and power-law fit on the *J-R* curve, J_c is the value corresponding to the intersection of an offset of the blunting line at Δa = 0.2 mm with the power-law fit on the J-R curve, whereas J_{szw} is the value

corresponding to stretch zone width on the *J-R* curve. Figure 6 shows the comparison of J_{szw} with J_i and J_c for 20MnMoNi55 and SA333 steels with change in *a/W* ratio. The stretch zone images for a low *a/W* (≈ 0.25) and a high *a/W* (≈0.76) in 20MnMoNi55 steel are shown in Fig.7.

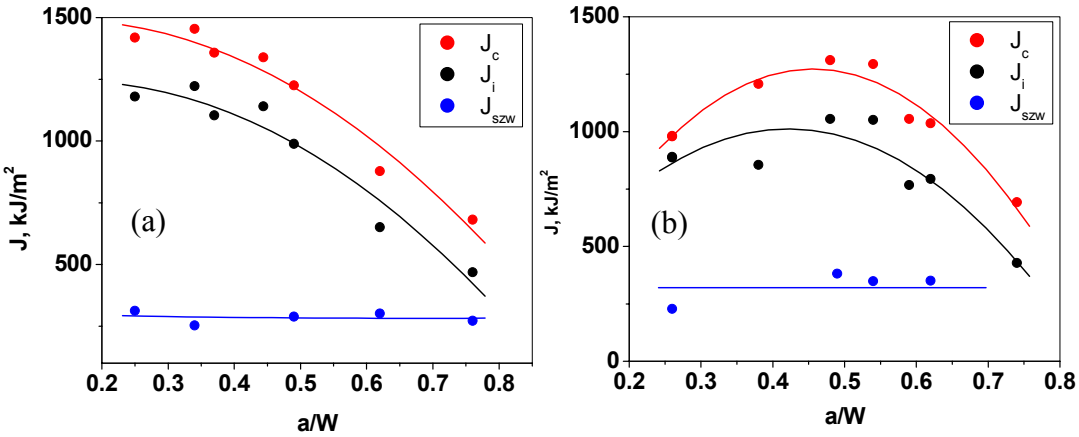

Fig. 6 Variation of J_i and J_c and J_{SZW} with change in *a/W* for (a) 20MnMoNi55 and (b) SA333 steels.

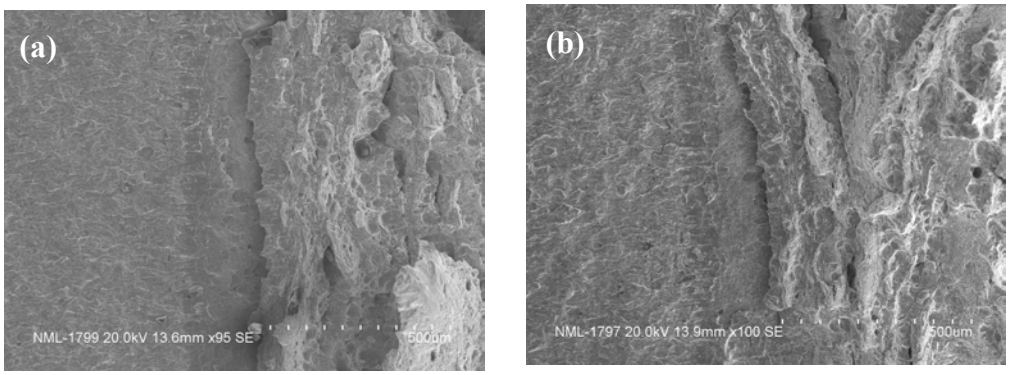

Fig. 7 The stretch zone images at different *a/W* for 20MnMoNi 55 steel: (a) a/W = 0.25, (b) a/W = 0.76

It is clear from Fig.6 that J_{szw} appears not to be affected by *a/W* (and thus constraint), and its value is much less than J_i and J_c values. The J_{szw} parameter, determined from stretch zone width, represents the fracture toughness of materials irrespective of the constraint condition to which cracks in them are subjected. The dimensions of the J_{szw} can therefore be correlated to the fracture toughness irrespective of the initial crack length (*a/W* ratio). Roos and Eisele [12] have also shown that the dimensions of the stretch zone can be correlated to fracture toughness irrespective of size and geometry of the specimen.

It was observed that J_{SZW} does not effect by a/W, and that its value is lower bound to J_i and J_c values for both the materials investigated. Sivaprasad *et al* have observed a similar phenomenon in HSLA steel [4]. The deviation of J_{SZW} from J_c could be due to several reasons. One of the possible reasons may be accuracy of crack length measured using the compliance method during crack tip blunting and at very small change in crack length. The second possibility is that J_c value is determined at 0.2 mm crack extension, while the J_{SZW} measurements were made at just before crack initiation, this could have given raise to the variation in the fracture toughness obtained by the two methods. Another reason could be effect stress triaxiality especially at lower a/W [5]. By changing crack length, the constraint condition at the crack tip gets vary, and that the stress field at the crack tip will deviate from the HRR field and may lead to higher fracture toughness.

4. Conclusions

(i) The initiation toughness, J_i, obtained at the intersection of the blunting line and the power-law fit to the *J-R* curve, and the critical toughness, J_c, determined following the procedure of the ASTM standard, exhibits sensitivity to crack tip constraint.

(ii) A loss of constraint enhances J_i and J_c values. These parameters are higher at lower a/W, i.e. under low constraint, and fall with increasing a/W.

(iii) It is observed that J_{SZW} (J value corresponding to stretch zone width) value is not sensitive to a/W, and therefore to constraint condition attending the crack tip. Further, its value is lower bound to J_i and J_c values for both the materials investigated.

References

1. M. T. Kirk, K. C. Koppenhoefer and C. F. Shih, Effect of Constraint on Specimen Dimensions Needed to Obtain Structurally Relevant Toughness Measures, in '*Constraint effects in fracture'*, ASTM STP 1171, Eds., E. M. Hackett, K-H. Schwalbe and R.H. Dodds, Philadelphia, PA, ASTM (1993) pp. 79-103.

2. R. K. V. Suresh, N. Ramakrishnan, M. Srinivas, P. Ramarao, On the determination of J(IC) using the stretch zone width method, *J. Testing and Evaluation,* **27** (1999) 211-218.

3. S. V. Kamat, M. Srinivas, P Rama Rao, On measuring mixed mode I/III fracture toughness of ductile materials using the critical stretch zone width, *J. Testing and Evaluation,* **34** (2006) 111-120.

4. S. Sivaprasad, S. Tarafder, V. R. Ranganath, S. K. Das and K. K. Ray, Effect of prestrain on stretch zone formation during ductile fracture of Cu-strengthened high strength low alloy steels, *Met. Mater. Trans A*, **33** (2002) 3731-3740.

5. S. Tarafder, V. R. Ranganath, S. Sivaprasad and P. Johri, Ductile fracture behaviour ofprimary heat transport piping material of nclear reactors, *Sadhana*, **28** (2003) 167-186.

6. ASTM: 'Standard test method for measurement of fracture toughness', E1820-99a, Philadelphia, PA, ASTM, 2000.

7. James A Joyce and Richard E Link, Application of two parameter elastic-plastic fracture mechanics to analysis of structures, *Engg. Fracture Mechanics*, **57** (1997), 431-446.

8. J.D.G. Sumpter, J_c determination for shallow notch welded bend specimens, *Fatigue & Fracture in Engg. Mats. & Struc.*, **10** (1987), 479-493.

9. J.D.G. Sumpter and A.T. Forbes, Constraint based analysis of shallow cracks in mild steel, *Proc. TWI/EWI/IS Int. Conf. On Shallow Crack Fracture Mechanics, Toughness Tests and Applications*, Cambridge, UK, September, 1992.

10. J.D.G. Sumpter, An experimental investigation of the T stress approach, Constraint Effects in Fracture, in *Constraint effects in fracture* ASTM STP1171, Eds., E.M. Hackett, K-H. Schwalbe and R.H. Dodds, ASTM Philadelphia, PA (1993), pp 492-502.

11. Y.J. Chao and W. Ji, Cleavage fracture quantified by J and A_2, in *Constraint effects in fracture theory and applications: Second Volume*, ASTM STP 1244, Eds., M. Kirk and A. Bakker, ASTM Philadelphia, PA (1995), pp.3-20.

12. E. Roos and U. Eisele, Determination of material characteristic values in elastic-plastic fracture mechanics by means of *J*-integral crack resistance curves, *J. Testing & Eval.*, **16** (1988), 1-11.